POLITECNICO DI TORINO
Repository ISTITUZIONALE

Quench propagation in a TF coil of the EU DEMO

Original
Quench propagation in a TF coil of the EU DEMO / Savoldi, Laura; Bonifetto, Roberto; Brighenti, Alberto; Corato, V.; Muzzi, L.; Turtu', S.; Zanino, Roberto; Zappatore, Andrea. - In: FUSION SCIENCE AND TECHNOLOGY. - ISSN 1943-7641. - STAMPA. - 72:3(2017), pp. 439-448. [10.1080/15361055.2017.1333866]

Availability:
This version is available at: 11583/2666647 since: 2018-01-23T00:51:28Z

Publisher:
American Nuclear Society

Published
DOI:10.1080/15361055.2017.1333866

Terms of use:

This article is made available under terms and conditions as specified in the corresponding bibliographic description in the repository

Publisher copyright
Taylor and Francis postprint/Author's Accepted Manuscript

This is an Accepted Manuscript of an article published by Taylor & Francis in FUSION SCIENCE AND TECHNOLOGY on 2017, available at http://wwww.tandfonline.com/10.1080/15361055.2017.1333866

(Article begins on next page)

18 December 2025

Quench propagation in a TF coil of the EU DEMO

L. Savoldi[1], R. Bonifetto[1], A. Brighenti[1], V. Corato[2], L. Muzzi[2], S. Turtu[2], R. Zanino[1,], A. Zappatore[1]*

[1]NEMO Group, Dipartimento Energia, Politecnico di Torino, Torino, Italy

[2]ENEA, Frascati, Italy

* Corresponding author: Roberto Zanino, mail address: *roberto.zanino@polito.it*, telephone number*: +39 011 090 4490*

Total number of pages: 25

Total number of tables: 2

Total number of figures: 10

Quench propagation in a TF coil of the EU DEMO

L. Savoldi, R. Bonifetto, A. Brighenti, V. Corato, L. Muzzi, S. Turtu', R. Zanino, A. Zappatore

Abstract

The design of a suitable quench protection system is fundamental for the safe operation of superconducting magnets and in turn requires the accurate simulation of the quench transient. The quench propagation in a toroidal field (TF) coil for the future European fusion reactor (EU DEMO) is analyzed here considering the latest, layer-wound winding pack (WP) design proposed by ENEA. The thermal-hydraulic model of a TF coil implemented in the 4C code is updated by including the external cryogenic circuits of the WP and of the casing cooling channels and proposing a preliminary layout of the quench lines. Three different locations are considered for the quench initiation: maximum temperature margin in the WP, and minimum and maximum temperature margin on the same turn of the innermost layer. The evolution of the main electrical and thermal-hydraulic parameters is simulated, such as voltage along each layer, quench front propagation both along and across the layers, hot spot temperature, pressurization of the coil and coolant mass flow rate at the coil boundaries, so that the 4C code provides a reliable (in view of its validation) and detailed virtual monitor of what happens inside the coil during the quench transient. In all cases considered, the ENEA design is predicted to satisfy the present (i.e., ITER) design criteria concerning the maximum allowed hot spot temperature.

Keywords: DEMO, superconducting magnets, quench

I. Introduction

After the 2015 design-base review, the toroidal field (TF) superconducting (SC) magnet system of the European fusion reactor (EU DEMO) consists of 18 coils where the winding pack (WP) is enclosed in a thick steel structure (the casing) that withstands the high electro-mechanical loads during operation.[1]

Three different WP proposals, by different groups (Commissariat à l'énergie atomique et aux énergies alternatives (CEA), Agenzia nazionale per le nuove tecnologie, l'energia e lo sviluppo economico sostenibile (ENEA) and Swiss Plasma Center (SPC)) inside the EUROfusion magnets work package (WPMAG), are being investigated from the mechanical, electrical and thermal-hydraulic point of view, in order to assess pros and cons of each proposal.[2]

Here we focus on the latest ENEA TF WP design consisting of 6 double-layers (DLs), see Fig. 1a, of which the first five, at the highest field, are graded in Nb_3Sn (and in the number of pure Cu strands), while the outermost uses NbTi, see table I. The reason/interest for the grading of the SC strands, see table I, is due to the distribution of the magnetic field on a cross section of the magnet, which is shown in Fig. 1b. The grading of the Cu area, see again table I, is instead based on adiabatic calculations of hotspot temperature. All layers are cooled in parallel by supercritical He flowing in counter-current in neighboring layers.[3] For each DL, a rectangular conductor is used, see Fig. 1c, with the peculiarity of two cooling channels, delimited by a spiral, instead of one as in the ITER conductors. These channels constitute the core of 2 of the 6 petals (the last-but-one cabling stage) and thus are twisted with them in the cable. The core of the other four petals, as well as the core of the last cabling stage, is constituted by a bundle of pure copper strands, also clearly visible in the picture, with a larger (1.5 mm) diameter with respect to the SC ones (1 mm). The turn and layer insulation thickness is 1 mm and 2 mm, respectively, resulting in a 2 mm and 4 mm thick G-10 glass epoxy insulation layer between adjacent turns and layers, respectively.[4] Note the jacket thickness increase from ~4 mm to ~12 mm (Fig. 1a) while moving radially from DL1.1 to DL6.2, due to structural reasons.

This paper is devoted to the study of quench propagation inside a TF coil, which is useful to assess the capability of the different WP designs to satisfy the corresponding design criteria, as well as to design a suitable quench protection system (QPS) for the coil.[5] In view of the complex 3D transient nature of the phenomenon, complex models and tools are needed to perform an accurate analysis. Here we use the 4C code,[6] developed at Politecnico di Torino for the analysis of thermal-hydraulic transients in superconducting magnets, which was recently used for a first modeling attempt of an EU DEMO TF coil,[7] after having been extensively validated against experimental data from different types of transient and different magnets and facilities, including the ITER Model and Insert coils,[8] the W7-X non-planar coils, the KSTAR and EAST magnet systems, and also applied to the ITER TF magnets.[9,10]

A first quench study for the 2014 ENEA WP design,[4] did not include the external cooling circuit of the WP, which is instead known to play a relevant role in the quench propagation,[11] nor the casing (the WP was considered adiabatic in correspondence of the ground insulation) with its casing cooling channels (CCCs).

In the present paper, a revised model of a TF coil is presented and implemented in the 4C code. The new model includes both the WP and the casing cooling loops,[7] and a preliminary layout of the quench lines is also proposed. In order to do that, we assume a schematic of the two cooling circuits as presented in Fig. 2. Notice that, considering the low pressure drop across the CCCs, only one safety valve is present in their cooling circuit, as opposed to the WP cooling circuit.

The scheme of the cryogenic circuit is derived from what is foreseen in the ITER: cryolines (i.e., pipelines outside the cryostat) and feeders (i.e., pipelines penetrating into the cryostat), while the He flow is forced by a centrifugal pump with a simple but realistic quadratic characteristic.[10] With respect to the circuit described in previous works,[7] a preliminary design of the quench lines has been added, based again on the ITER design: the opening of the safety valves (SV) is triggered by an overpressure of 2 MPa, at which time He is vented, through dedicated quench lines, inside the quench tanks (initially at atmospheric pressure);[10] the volume of the latter has been rescaled, with respect to the ITER design, according to the total volume of He in the DEMO TF coils.

The upgraded 4C model is applied to the analysis of the propagation of a quench initiated at the end of a plasma burn and different locations inside the coil. The evolution of the voltage across each layer and the propagation of the quench are computed together with the evolution of the main thermal-hydraulic parameters, such as hot spot temperature, mass flow rate and pressure at the coil boundaries, maximum pressure in the coil, temperature distribution in the structures, etc. The computed hot spot temperature (both jacket and strands) is finally compared with the currently prescribed limits in the ITER design criteria, which are currently adopted also for DEMO.[12]

II. 4C model of a DEMO TF coil

The 4C model of a DEMO TF coil includes

- *WP*, where 1D He flow along each CICC (layer) is coupled to 1D heat conduction along strands and jacket. A first quench study for the 2014 ENEA WP design,[4] demonstrated the relevance of the heat transfer between adjacent layers, not included in previous work.[13,14] Therefore, inter-turn and inter-layer thermal coupling are included in the model.
- *Casing*, poloidally discretized using "cuts", thermally-hydraulically coupled to the neighboring cuts by 1D He advection along each CCC and/or WP layer. 2D heat conduction on each cut is assumed and modeled, coupled to the flow in the CICC and CCC.[7]
- *External cryogenic circuits*, described using an ad-hoc developed Modelica library of components (circulator, HX, cryolines, valves, …), separately validated in a series of both interpretive and predictive exercises,[15] by comparison with experimental data from the HELIOS facility at CEA Grenoble.

III. Simulation setup

In Fig. 3 the different phases of a single cycle foreseen for DEMO pulsed operation are reported. After the initial phases of Poloidal Field (PF) coils charge and plasma current ramp-up, where AC losses are induced in the TF coils by current variations in other magnet systems, a short (~10 s) external heating by neutral beam

injection and radiofrequency will start the burn phase. During the plasma burn, lasting ~2 h, the current adjustments in Central Solenoid (CS) and PF coils will still induce some AC losses in the TF magnets, which will also be subject to the nuclear heat load from fusion reactions in the plasma. At the end of the flat-top (EoF) of the plasma current, the shutdown of the PF coils will induce again AC losses in the TF coils. A dwell time of ~1/2 hour will follow, before the start of a new cycle.

A simulation of a series of 9100 s plasma pulses is performed first until a periodic behavior is reached, in order to determine the spatial distribution of the temperature margin inside the coil.[3] In this simulation, according to Fig. 3, the nuclear heat load (exponentially decreasing in space with the distance from the inner coil side) is applied only during the 2-hour plasma shot. AC losses and eddy current losses due to CS and PF current variations, as well as the static heat load, are presently not accounted for in the model.

Starting from the EoF conditions, the quench transient is then initiated by a thermal disturbance equal to the (computationally estimated) Minimum Quench Energy and applied for 0.1 s on a 0.1 m long region,[4,12] the so-called initial normal zone (INZ), centered at three relevant locations (see Fig. 4):

- Case α: quench initiated at the location of the maximum margin ΔT_{marg}^{max} (~9 K) on the outermost Nb3Sn layer (x_{inz} ~357 m from the inlet of DL5.2); this is the location where, due to the slower propagation speed because of the high temperature margin, the hot spot temperature is in principle expected to be maximum
- Case β: quench initiated at the location of the minimum margin ΔT_{marg}^{min} (~2 K) on the innermost layer (x_{inz} ~504 m from the inlet of DL1.1); experiencing the maximum values of magnetic field and nuclear heat load, it is the DL where a quench initiation due to a field or heat load perturbation is more likely.
- Case γ: quench initiated at the location of the maximum margin ΔT_{marg}^{max} (~5 K) on the innermost layer (x_{inz} ~486 m from the inlet of DL1.1), in the same turn where the minimum margin (case β) is also located; this is very close to the maximum temperature margin on DL1.1, which is located at the inlet and is therefore not relevant for the comparison with the other cases.

The choice of the first two cases follows the WPMAG guidelines,[12] i.e., considering as quench initiation locations the maximum and minimum margin locations *over the whole winding*.[a] The rationale of this guideline is that at the minimum margin location the quench initiation should be most likely, whereas a quench initiated at the maximum margin location could lead to the highest hot spot temperature because of the lowest propagation speed and resulting delay in the quench detection. The latter reason motivates the analysis of case γ, which *in principle* is expected to lead to the maximum hot spot temperature on DL1.1.

The current dump from the nominal 70.8 kA is triggered 1.1 s after the voltage on a single layer reaches the quench detection threshold of 0.1 V,[12] see Fig. 3. During the dump, the coupling losses (W/m) in all DLs are assumed to follow the simple, single time constant behavior:

$$\dot{Q}_{lin}(x,t) = \frac{n\tau}{\mu}\left\{\frac{B_0(x)}{I_0}\left[\frac{I_0}{\tau_{dump}}\exp\left(-\frac{t}{\tau_{dump}}\right)\right]\right\}^2 A_{st} \quad (1)$$

[a] Case β does not strictly speaking consider as quench initiation location that of the minimum margin across the whole coil, since the latter occurs in DL6.1. However, we refrain here to consider this case in alternative or even additionally to case β, because of several reasons: 1) the location of the INZ should be in this case very close to the DL outlet, whose effect on the quench propagation could be very difficult to assess reliably, so that basically only the upstream propagation should be effective; 2) the quench propagation in a NbTi CICC, even those of ITER with a single channel, is rather difficult to predict, especially in its initial phase, as NbTi CICCs are characterized by a premature voltage take-off if compared with that expected from the single strand performance,[16] related to the strong dependence of the critical current density on the magnetic field, coupled with the large magnetic field gradients present on the cross section of large conductors such as those of ITER.[17] Therefore, a coupled thermal-hydraulic/electromagnetic model is needed to account for current redistribution as well as temperature non-uniformities at sub-cable levels. [18]

where $n\tau$ = 1.35 s is the coupling time constant, μ is the permeability of the magnetic field in vacuum, A_{st} the SC strands cross section, $B_0(x)$ is the (initial) magnetic field distribution at full current I_0, τ_{dump} is the current decay constant (27 s) and t is the time measured from the start of the current dump.

Eddy currents in the casing are also accounted for, with the corresponding losses (MW) assumed to be uniformly distributed in space and to follow in time the exponential decay,[19]

$$\dot{Q}_{casing}(t) = 47.41 \exp(-0.06762t) \quad (2)$$

The initial mass flow rate circulated by the WP and CCCs pumps are ~60 g/s (~1/2 of ITER nominal value, due to an almost double channel length and reduced conductor void fraction) and ~150 g/s (~equal to ITER), respectively, with a Δp of ~1 bar in all cases.[12]

IV. Results

Table II summarizes the results concerning the hot spot temperature, comparing the three locations selected for the INZ. All cases are predicted to satisfy the design criteria of maximum jacket temperature below 150 K,[12] and maximum strand temperature below 250 K. Case β is more critical than case α from the hot spot temperature point of view, which can be explained by at least three different factors:

- first of all, the grading of the Cu (and SC) strands results in a Cu area increase by ~10% from DL1.1 to DL5.2; the additional Cu area reduces the hot spot temperature in the outer DLs;
- the jacket cross section in DL5.2 is ~2.5 times larger than in DL1.1, see the different thickness in Fig.1a; being the jacket heat capacity at relatively high temperature (~100 K) ~2 orders of magnitude larger than that of the He, the jacket thickness grading (due to structural reasons) provides, as a fringe benefit, a higher thermal capacity in DL5.2, contributing to reduce the hot spot temperature, as already noted elsewhere;[20]

- the higher magnetic field in DL1.1 also results in an increase of the copper wires magnetoresistance, partially contributing to the temperature increase in the hot spot region of the inner DLs.

While the impact of the magnetoresistance variation is small (less than ~3 K), the major role is played by the two other factors, which are almost equally responsible for the hot spot temperature reduction in DL5.2. Case γ, besides being in practice less relevant than case β (it should require a much higher minimum quench energy deposition, which is unlikely because of the relatively uniform energy deposition expected on DL1.1), will not result in a higher hot spot temperature, if compared to case β, because:

- the maximum margin on DL1.1 is only ~twice the minimum margin, so that the initial propagation speed is almost equal to that of case β, resulting in a comparable detection time, but with a smaller heat deposition;
- in the high field (low margin) region, the cooling of the cable by conduction is smaller, being the Cu thermal conductivity ~40% smaller at higher magnetic field.

In the following, we will therefore concentrate on case β.

The evolution of the voltage across the DL1.1 is shown in Fig. 5a, together with the cable hot spot temperature evolution. While the latter presents a smooth increase in time, up to the hot spot of ~120 K (reached at ~35 s), the voltage shows several slope changes at the times when the quench propagates by conduction across the jacket and the turn insulation to adjacent turns, see the quench front propagation in DL1.1 reported in Fig. 5b. Over a similar time scale, inter-layer heat diffusion leads to the quench initiation also in neighboring layers, as shown in Fig. 5b for DL1.2 and DL2.1, as the inter-layer thermal resistance is ~2× the inter-turn one (due to the ~2× thicker insulation thickness, see above), but is compensated by the contact length, which is also ~2× larger in the case of inter-layer thermal coupling, see Fig. 1a. The quench detection threshold of 0.1 V is overcome in DL1.1 at 2.1 s, and the dump is then triggered at 3.2 s. The normal zone propagation is accelerated

by the AC losses induced by the current dump, as it can be seen in DL1.1 both in Fig. 5b and from the voltage evolution in Fig. 5a.

The effect of inter-turn and inter-layer coupling is clearly visible in Fig. 6: the quench is induced in turn 12 of DL1.1 (a) and then it propagates to the adjacent turns (b) and almost at the same time also to adjacent layers (c), (d) and (e).

The pressure at the conductor boundaries starts increasing at the dump, when the AC losses start generating power along the whole cable length, see Fig. 7a; at this time the outlet mass flow rate suddenly increases and the inlet mass flow rate undergoes back flow, as shown in Fig. 7b. The interest for the latter is related to the fact that the secondary quench detection system in ITER is based on the mass flow rate / backflow measurement at the conductor inlet,[21] even though additional, on-purpose analyses are required to better judge the effectiveness of such a secondary quench detection (e.g. undetected quenches to assess the effect of the quench without the AC losses due to the current dump). The slope of the pressure and of the mass flow rate evolution changes when the quench is initiated in neighboring turns and the pressure in the conductor continues to increase until, as a consequence of the high energy deposited in the DL1.1 by Joule heating (one order of magnitude higher than AC losses, see Fig. 8), it reaches a peak of ~6.4 MPa, which is well below the maximum acceptable pressure according to the current DEMO design criteria, assumed at present to be the same as the ITER ones (25 MPa). During the simulated transient, the inlet and outlet pressures stay both below the 2 MPa threshold for the opening of the SV in the WP circuit (this feature is of course strictly related to the assumed He volume in the circuit, but on the other hand the detailed circuit design is well beyond the scope of the present work). After the last increase at ~30 s, when the quench is initiated also in the last turn, the outlet mass flow rate starts to decrease, see Fig. 7b, due to the reduced He density in the conductor.

In Fig. 7b also the mass flow rate at the inlet and outlet of DL3.1 is shown. It is seen that in the initial phase the AC losses lead to He expansion in all DLs and therefore to backflow of the He also at the inlet of DL3.1, although the quench there has not been initiated yet, see Fig. 6. However, after the AC loss power is sufficiently decreased, the pressurization of the common inlet and outlet manifold induced by the quenched DL causes a mass flow rate *increase* at the inlet and dm/dt *decrease*/reverse flow at the outlet of neighboring layers,

e.g. DL3.1 at ~10 s, and therefore it can lead to a possible initiation of the quench in these, due to the inflow of warm He from the quenched DLs, see Fig. 7b.

After the dump, the power deposition by eddy currents in the structures, see Fig.8, induces a fast temperature increase in the casing, see Fig.9, and a strong pressurization of the He in the CCCs, see Fig. 10a, which leads to the opening of the SV in the casing cooling loop and to backflow at the CCCs inlet. The thick (~2 cm) insulation between the casing and the WP is able to prevent a fast heating of the latter, even if the high temperature gradient on the insulation layer, see the insets in Fig. 9, can be of a concern as it may crack or exfoliate.

Helium is discharged in the quench tank and after ~35 s, the total helium mass vented is ~15 kg, corresponding to ~32% of the total He inventory in the casing cooling circuit, see Fig. 10b. The mass flow rate change at ~32 s is synchronized with the time at which the pressure upstream the pump becomes lower than downstream. The higher pressurization at the outlet of the CCCs is due to the fact that the SV in the casing cooling loop is located at the inlet of the CCCs.

V. Conclusions

The quench initiated at three different locations in a superconducting TF coil of the EU DEMO fusion reactor adopting the latest ENEA WP design has been studied using the 4C thermal-hydraulic code.

The model is rather comprehensive and includes the 1D flow of SHe in each of the thermally coupled layers of the WP and in the casing cooling channels, the quasi 3D heat conduction in the casing, the external cryogenic circuits for both WP and casing with quench lines. Based on this, and on the level of validation of the 4C code, it can be claimed that a detailed and reliable (computational) monitoring of what happens in the coil is possible.

The model accounts for both eddy currents heat deposition in the casing and AC losses in the cable induced by the fast discharge triggered by the quench protection system.

Both the maximum jacket hot spot temperature and the maximum pressure reached during the quench are predicted to stay below the presently (= ITER) prescribed limits. The highest hot spot temperature is reached when the quench is initiated at the minimum temperature margin location in DL1.1, mainly due to the Cu area grading, as well as to the different jacket thickness in the different DLs. This suggests that future analyses should also address the localization of the most critical quench initiation position, from the hot spot temperature point of view, which does not necessarily coincide with the maximum margin location in a layer-wound WP.

The power deposition in the casing induced by eddy currents during the dump induces a pressurization of the casing cooling circuit leading to the opening of the safety valves with consequent venting of ~1/3 of the total He inventory in the casing cooling circuit.

Acknowledgements

This work has been carried out within the framework of the EUROfusion Consortium and has received funding from the Euratom research and training programme 2014-2018 under grant agreement No 633053. The views and opinions expressed herein do not necessarily reflect those of the European Commission. The work of RB is financially supported by a EUROfusion Engineering Grant. The PhD fellowship of AB is partially funded by EUROfusion.

The authors thank the two anonymous reviewers for comments that led to a significant improvement of the paper.

References

[1] EU DEMO1 2015 Demo tokamak complex, 2015, https://idm.euro-fusion.org/?uid=2M9AJJ.

[2] L. ZANI, et al., "Overview of Progress on the EU DEMO Reactor Magnet System Design," *IEEE Trans. Appl. Supercond.*, vol. **26**, no. 4, Art. ID 4204505, Jun. (2016).

[3] L. SAVOLDI, et al., "Performance Analysis of a Graded Winding Pack Design for the EU DEMO TF Coil in Normal and Off-Normal Conditions," submitted to *Fus. Eng. Des.* (2016).

[4] L. SAVOLDI, et al., "Analyses of Low- and High-Margin Quench Propagation in the European DEMO TF Coil Winding Pack," *IEEE Trans. Plasma Science*, vol. **44**, no. 9, (2016).

[5] A. MAISTRELLO, and E. GAIO, "Studies on the TF Circuit of DEMO," EFDA_D_2M8RJB v1.0, 29/01/2016.

[6] L. SAVOLDI RICHARD, et al., "The 4C Code for the Cryogenic Circuit Conductor and Coil Modeling in ITER," *Cryogenics*, vol. **50**, no. 3, pp. 167-176, Mar. (2010).

[7] R. ZANINO, et al., "Development of a Thermal-Hydraulic Model for the European DEMO TF Coil," *IEEE Trans. Appl. Supercond.*, vol. **26**, no. 3, Art. ID 4201606, Apr. (2016).

[8] R. BONIFETTO, et al.. "Analysis of Quench Propagation in the ITER Central Solenoid Insert (CSI) Coil," to appear in *IEEE Trans. Appl. Supercond*, (2016), DOI: 10.1109/TASC.2016.2634598.

[9] R. ZANINO, et al., "Quench Analysis of an ITER TF Coil," *Fus. Eng. Des.*, vol. **85**, no. 5, pp. 752-760, Aug. (2010).

[10] L. SAVOLDI RICHARD, et al., "Parametric Analysis of the ITER TF Fast Discharge Using the 4C Code," *IEEE Trans. Appl. Supercond.*, vol. **22**, no. 3, Art. ID 4704104, Jun. (2012).

[11] C. MARINUCCI, et al., "The Hydraulic Solver Flower and Its Validation Against the QUELL Experiment in SULTAN," *IEEE Trans. Appl. Supercond.*, vol. **9**, pp. 616-619, Jun. (1999).

[12] K. SEDLAK, et al., "Common Operating Values for DEMO Magnets Design for 2016," EFDA_D_2MMDTG v1.4, 21/06/2016.

[13] R. VALLCORBA, et al., "Thermo-hydraulic Analyses Associated With a CEA Design Proposal for a DEMO TF Conductor," *Cryogenics*, vol. **80**, no. 3, p. 317-24, (2016).

[14] M. LEWANDOWSKA, et al., "Thermal-Hydraulic Analysis of the Low-T_c Superconductor (LTS) Winding Pack Design Concepts for the DEMO Toroidal Field (TF) Coil," *IEEE Trans. Appl. Supercond.*, vol. **26**, no. 4, Art. ID 4205305, Jun. (2016).

[15] R. ZANINO, et al., "Verification of the Predictive Capabilities of the 4C Code Cryogenic Circuit Model," *AIP Conf. Proc.*, vol. **1573**, pp. 1586-1593, (2014).

[16] P. BRUZZONE et al., "Test Results of the ITER PF Insert Conductor Short Sample in SULTAN", *IEEE Trans. Appl. Supercond.*, vol. **15**, pp. 1351-4, (2005).

[17] R. ZANINO et al., "Analysis of Quench Propagation in the ITER Poloidal Field Conductor Insert (PFCI)", *IEEE Trans. Appl. Supercond.*, vol. **20**, no. 3, (2010).

[18] R. ZANINO et al., "Analysis of Sudden Quench of an ITER Superconducting NbTi Full-Size Short Sample Using the THELMA Code", *Supercond. Sci. Technol*, vol. **24**, no. 10, (2011).

[19] A. TORRE, "Proposal for Eddy Currents Calculation in DEMO TF Coils Casing Elements During Fast Discharge", EFDA_D_2MB7BY, 17/05/2016.

[20] K. SEDLAK, and P. BRUZZONE, "Results and Aanalysis of the Hot-Spot Temperature Experiment for a Cable-In-Conduit Conductor With Thick Conduit," *Cryogenics*, vol. **72**, no. 1, pp. 9-13, Mar. (2015).

[21] S. NICOLLET, et al., "Thermal Behavior and Quench of the ITER TF System During a Fast Discharge and Possibility of a Secondary Quench Detection," *IEEE Trans. Appl. Supercond.*, vol. **22**, no. 3, Art. ID 4704304, Jun. (2012).

TABLE I. Main parameters of the newest ENEA TF WP DLs

	DL 1.1	**DL 1.2**	**DL 2.1**	**DL 2.2**	**DL 3.1**	**DL 3.2**	**DL 4.1**	**DL 4.2**	**DL 5.1**	**DL 5.2**	**DL 6.1**	**DL 6.2**
Length [m]	746.8	750.7	755.0	759.2	763.5	768.1	772.8	777.8	782.9	788.3	794.1	706.1
# SC strands	720		360		270		180		120		972	
Cu / non Cu ratio	1		1		1		1		1		1.6	
# Cu strands (ϕ = 1 mm)	360		720		540		630		960		0	
# Cu strands (ϕ = 1.5 mm)	108		54		162		108		0		108	

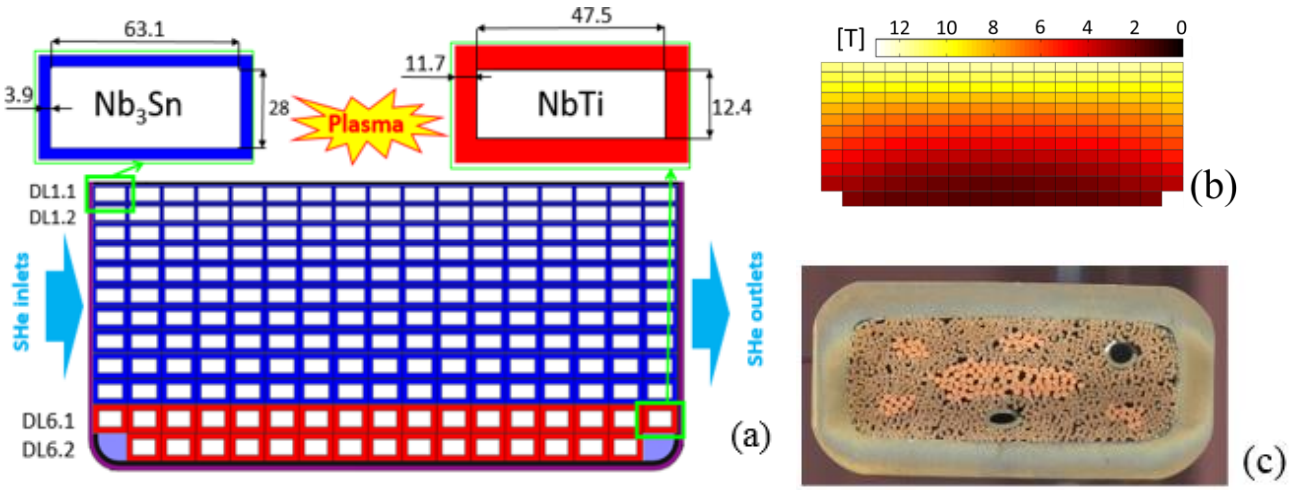

Fig. 1. (a) Sketch of the ENEA 2016 EU DEMO TF WP, layer-wound using 6 double layers (DL). The size (in mm) of the graded conductor used in DL1.1 and DL6.1 is also shown. (b) Example of computed magnetic field map on the WP cross section. (c) A picture of the cross section of the TF short sample: the 2 relief channels, delimited by a stainless steel spiral, are clearly visible.

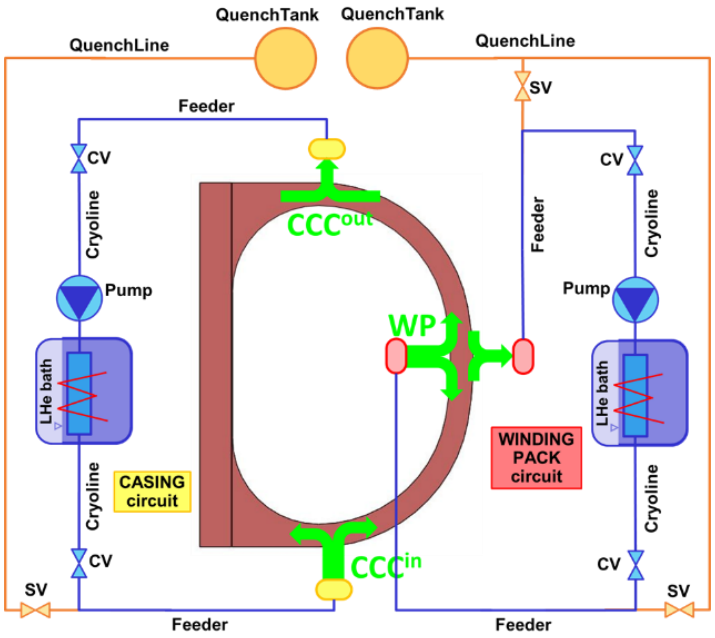

Fig. 2. Sketch of the TF cooling circuits (CV = control valve, SV = safety valve, LHe = liquid He).

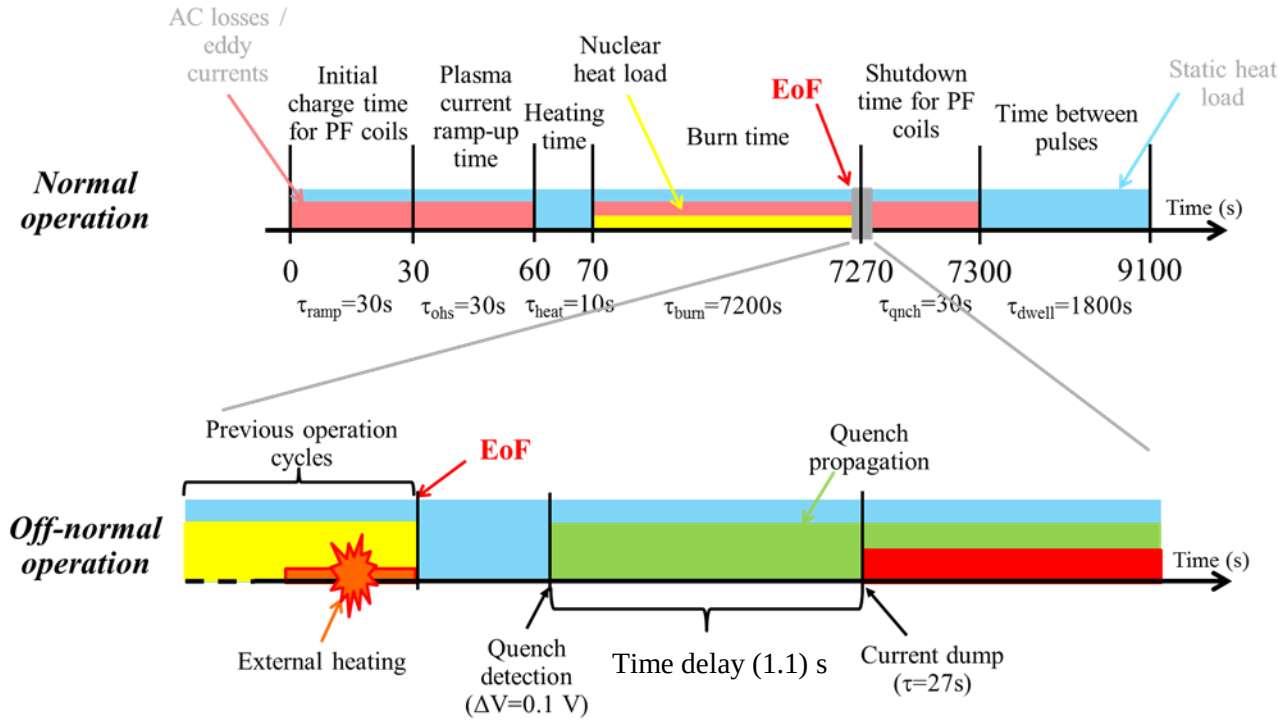

Fig. 3. Timeline of a 9100 s EU DEMO plasma pulse (normal operation, top), with the corresponding thermal loads. The quench transient analyzed in this work is initiated at EoF and reported in detail in the off-normal operation timeline (bottom).

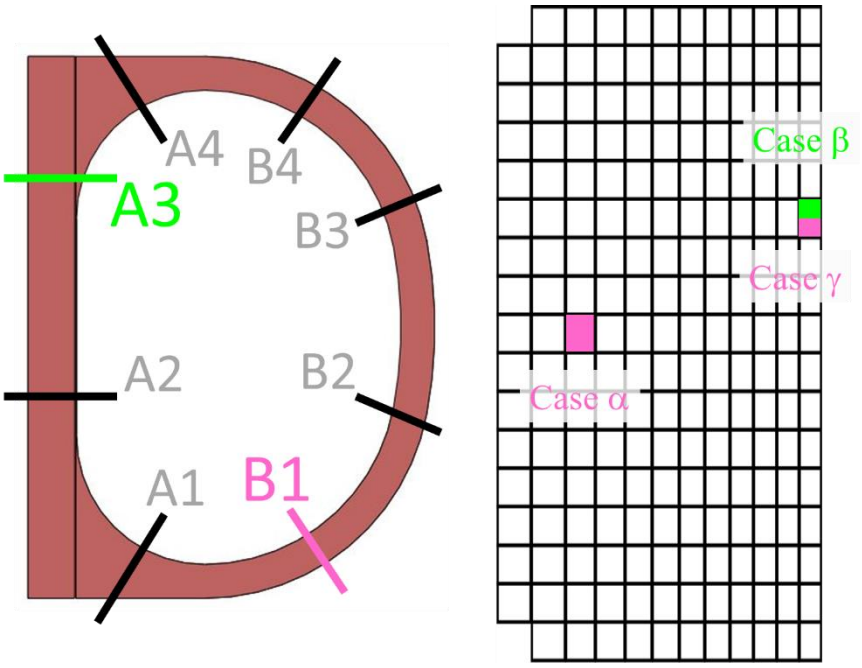

Fig. 4. Identification of the poloidal cuts (left) and position in the WP cross section (right) where the quench is initiated in the three cases considered in this paper (the color code explains also the poloidal location of the quench initiation in the left figure).

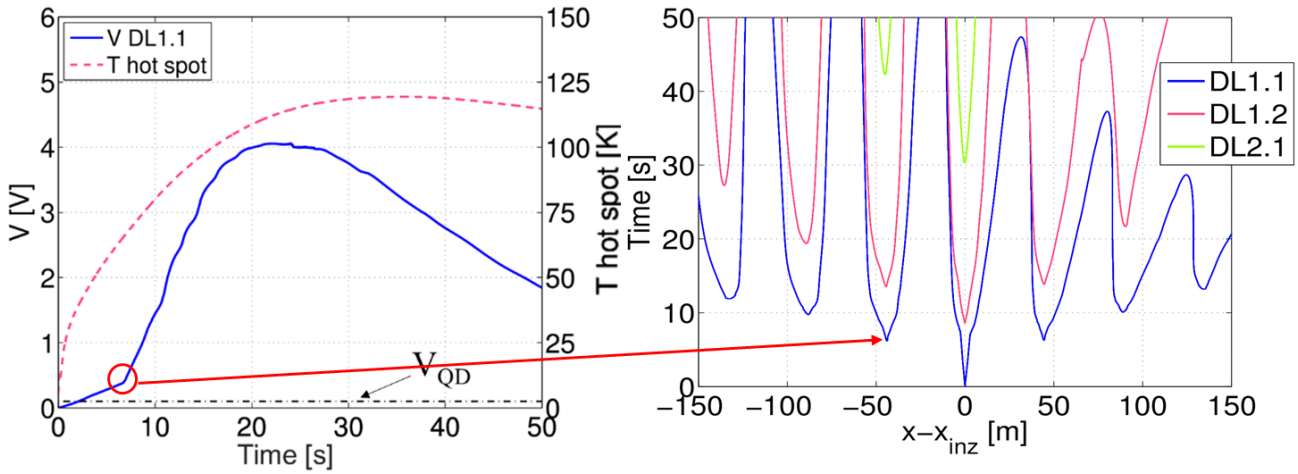

Fig. 5. Case β. (a) Evolution of voltage along DL1.1 (blue line, left y axis), and hot spot temperature (red line, right y axis). The level of the quench detection voltage is also indicated (dash-dotted line). (b) Quench front propagation in different DLs (different colors), described by the instantaneous location of the different quench fronts: the region between the two branches of each parabola identifies the instantaneous location of the NZ.

TABLE II. Estimated hot spot temperature in the coil and maximum jacket temperature.

Case	**Condition**	$T_{\text{hot spot}}$ **[K]**	$T_{\text{max,jk}}$ **[K]**
α	ΔT_{marg}^{max}, DL5.2	101	72
β	ΔT_{marg}^{min}, DL1.1	120	107
γ	ΔT_{marg}^{max}, DL1.1	110	96

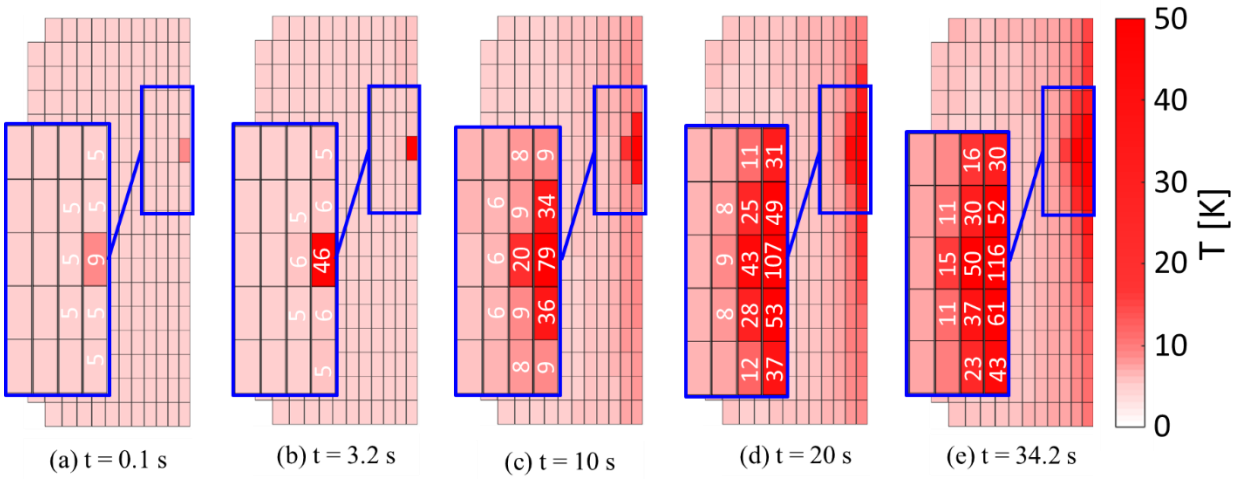

Fig 6. Case β. Evolution of the temperature distribution on the WP cross section at x_{inz}, showing the effects of inter-turn and inter-layer thermal coupling on the quench propagation. The maximum temperature values in the strands in selected turns are indicated in the zooms.

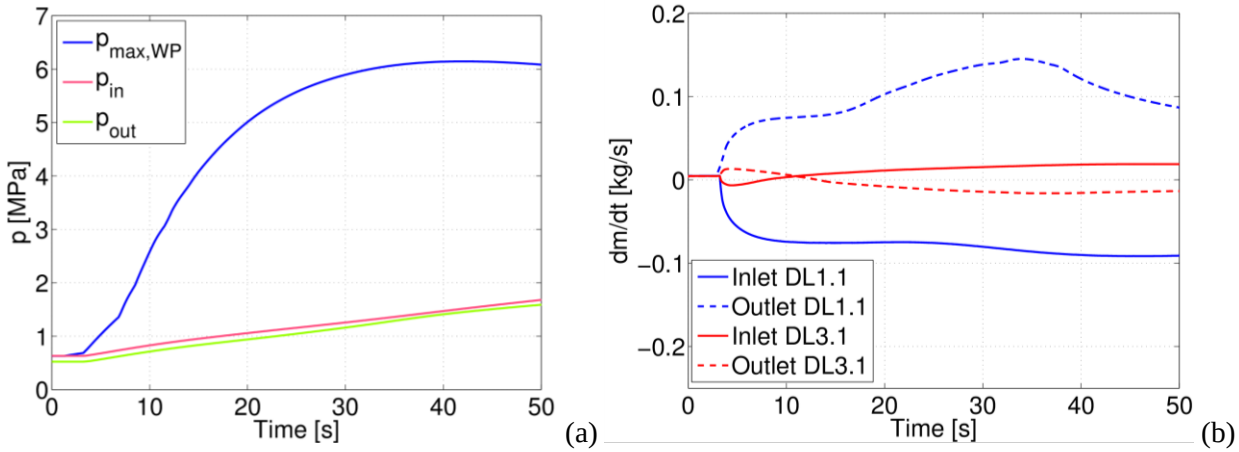

Fig. 7. Case β. (a) Maximum He pressure in the conductor (blue) and pressure at the boundaries (pink → inlet, green → outlet). (b) Mass flow rate in DL1.1 (solid blue → inlet, dashed blue → outlet) and DL 3.1 (solid red → inlet, dashed red → outlet), respectively.

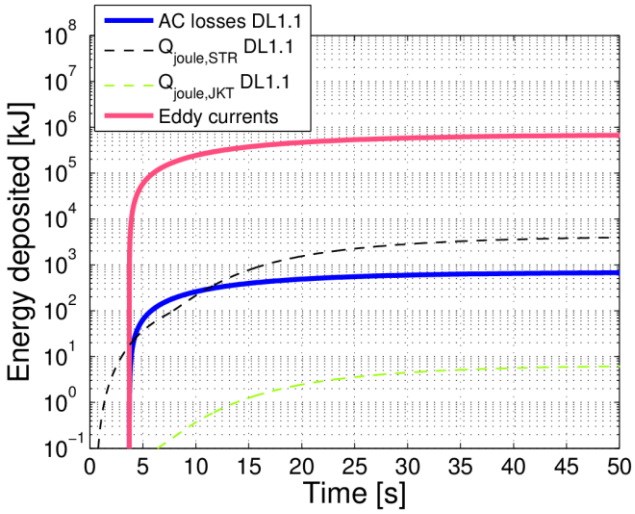

Fig. 8. Evolution of the energy deposited in DL1.1 due to AC losses (thick solid blue), Joule heating in strands (thin dashed black) and in jacket (thin dashed green), compared with the energy deposited in the casing by eddy currents (thick solid pink).

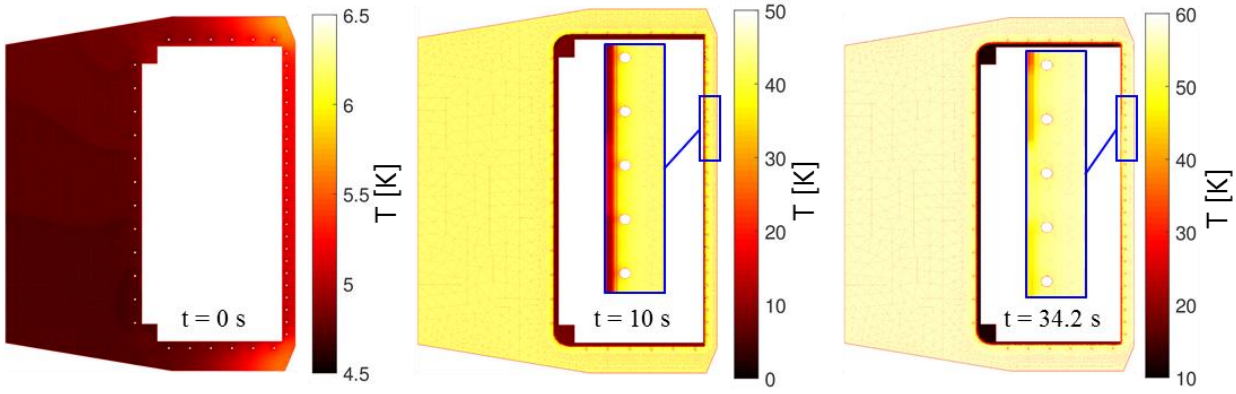

Fig. 9. 2D casing temperature map at different times on the A3 cut, i.e., at the poloidal location of x_{inz} for case β. The zoom around x_{inz} is reported in the insets.

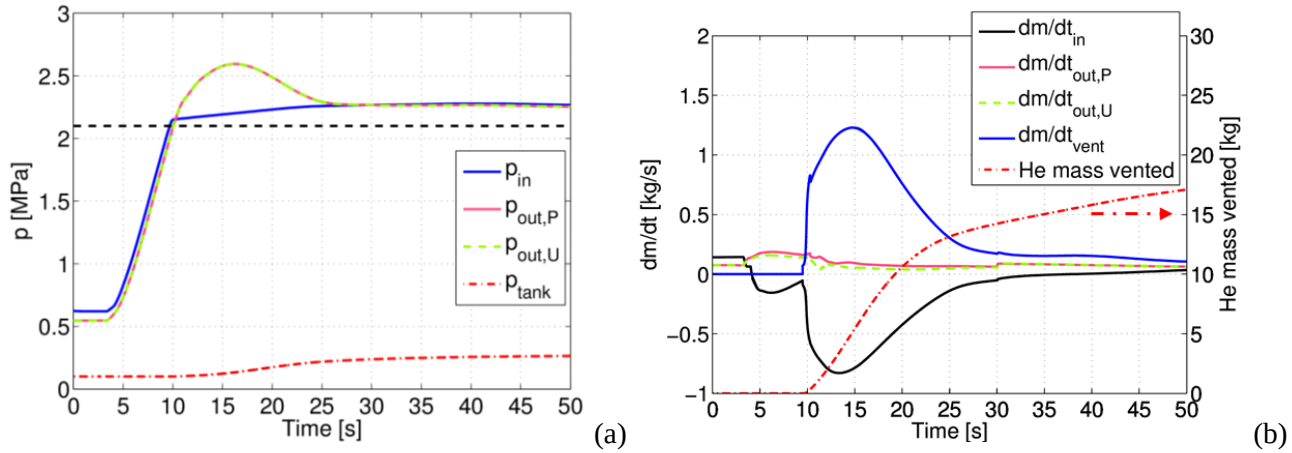

Fig. 10. (a) Inlet (solid blue) and outlet (solid pink line: plasma facing wall CCCs; dashed green line: back and side walls CCCs), pressure in the quench tank (red dashed-dot) is also shown. (b) Mass flow evolution at CCCs inlet (solid black line) and outlet (solid pink line: plasma facing wall CCCs; dashed green line: back and side walls CCCs), for case β. The mass flow rate vented through the SV (solid blue line) and the total mass vented (dash-dotted red line, right y axis) are also reported.